High energy electrons, nuclear phenomena and heating in petawatt laser-solid experiments

By T.E. COWAN,* M.D. PERRY,* M.H. KEY,*
T.R. DITMIRE,* S.P. HATCHETT,* E.A. HENRY,*
J.D. MOODY,* M.J. MORAN,* D.M. PENNINGTON,*
T.W. PHILLIPS,* T.C. SANGSTER,* J.A. SEFCIK,*
M.S. SINGH,* R.A. SNAVELY,* M.A. STOYER,*
S.C. WILKS,* P.E. YOUNG,* Y. TAKAHASHI,**
B. DONG,** W. FOUNTAIN,† T. PARNELL,†
J. JOHNSON,†† A.W. HUNT,§ AND T. KÜHL§§

*Lawrence Livermore National Laboratory, Livermore, CA, USA 94550
**University of Alabama, Huntsville, AL, USA 35899
†George C. Marshall Space Flight Center, Huntsville, AL, USA 35899
††University Space Research Association, Huntsville, AL, USA 35806
§Harvard University, Cambridge, MA, USA
§§Gesellschaft für Schwerionenforschung, Darmstadt, Germany

The Petawatt laser at Lawrence Livermore National Laboratory (LLNL) has opened a new regime of laser matter interactions in which the quiver motion of plasma electrons is fully relativistic with energies extending well above the threshold for nuclear processes. In addition to ~few MeV ponderomotive electrons produced in ultra intense laser-solid interactions, we have found a high energy component of electrons extending to ~100 MeV apparently from relativistic selffocusing and plasma acceleration in the underdense preformed plasma. The generation of hard bremsstrahlung, photonuclear reactions, and preliminary evidence for positron-electron pair production will be discussed.

1. Introduction

With the advent of high power, chirped-pulse amplification laser systems at a variety of laboratories, it has now become possible to produce highly relativistic laser plasmas. These offer the possibility of very short pulse, high-energy electron and secondary radiation sources for a variety of investigations beyond tests of the fast ignition concept for which these lasers were originally developed. For example, the prospect of producing very high energy electrons and bremsstrahlung, and subsequent nuclear reactions, was discussed in great detail at this conference (Meyer-ter-vehn 1998).

With the petawatt laser (Perry 1996) at Lawrence Livermore National Laboratory, the experimental observation of these effects has become possible for the first time. Developed primarily for ICF research (Key 1998), the petawatt uses one arm of the NOVA Nd:glass laser chain to amplify a frequency-chirped pulse to kJ energies before temporal compression to ~450 fs in a vacuum compressor using very large (94-cm-diameter) gratings. The peak power is well in excess of 1000 TW, and the 58-cm-diameter beam can be focused with an 80-cm-diameter f/3 on axis parabola to a <20-μm spot, with intensity exceeding 10^{20} W/cm^2. At these extreme intensities, the electromagnetic fields at the laser focus are enormous ($E > 10^{13}$

V/m, and $B > 10^5$ Tesla) and the motion of the electrons in the target plasma is fully relativistic. The cycle-averaged oscillation or "quiver" energy of the electrons,

$$\bar{E} = mc^2[1 + 2U_p/mc^2]^{1/2},\qquad(1)$$

can exceed several MeV, where $U_p = 9.33 \times 10^{-14}I$ (W/cm^2)$\lambda^2(\mu$m) is the nonrelativistic ponderomotive potential. The resulting distribution of electron energies in the target is predicted to resemble a Maxwellian (Wilks 1992), with mean energy given by equation (1), and it extends far beyond the threshold for which nuclear effects become important. An adjustable prepulse, at 2 or 10 ns before the main pulse and with an amplitude tunable over 10^{-4} to 10^{-1} of the peak energy, is used to preform an underdense plasma on the face of a solid target. This provides a medium in which to relativistically selffocus the laser beam to higher intensity, to increase the ponderomotive energies, and to produce selfmodulated wakefield acceleration of electrons to even higher energies (see e.g., Pukhov 1998 & Wilks 1998). The resulting bremsstrahlung cascade in the solid target produces high energy bremsstrahlung, positron-electron pairs, and photonuclear reactions in the target material. In this contribution we describe our first ultraintense laser-solid experiments with the petawatt, in which we observed 100-MeV electrons, photonuclear reactions, and a variety of relativistic laser-plasma effects.

2. High-energy electron spectroscopy at the petawatt

To characterize the entire electron energy range of interest, from few MeV ponderomotive electrons to several hundred MeV or GeV-scale plasma-accelerated electrons, we have fielded two types of compact, permanent magnet electron spectrometers (Cowan 1998a; Cowan 1998d) as shown in figure 1. The "low-energy" spectrometers, covering the electron energy range of 0.2 to 100 MeV, are mounted at 30° and 95° with respect to the laser beam incident on the target. The Nd-Fe-B permanent magnet material is sufficient to attain a field strength of 5.5 kG, over a 10-cm × 15-cm pole face dimension with a 3.8-cm gap. The electrons are recorded in nuclear emulsion track detectors which are positioned in the gap of the magnet such that the electron angle of incidence is a constant value of 10° throughout the dispersion plane. The emulsions consist of two layers of 50-μm-thick, fine grained silver bromide emulsion coated on the front and back surface of a 500-μm polystyrene strip. Microscopic examination of the developed emulsion strips allows clear identification of charged particle tracks and distinguishes electrons emitted from the target by virtue of the density of exposed grains along the track, the angle of incidence, and the transverse position along the emulsion strip (which must be within the image of the entrance aperture). A second emulsion strip in each spectrometer is oriented to detect positrons within the energy range of 0.2 to 40 MeV. Below about 2 MeV, however, both electrons and positrons undergo sufficient multiple scattering in the emulsion that the incidence angle and track length cannot be unambiguously determined and therefore cannot be distinguished from Compton electrons generated in the emulsions by the large flux of hard X-ray bremsstrahlung present in the solid target experiments.

The "high energy" spectrometer, designed for laser wakefield acceleration measurements (Cowan 1997; Cowan 1998b), covers an electron energy range of 100 MeV to 2 GeV. It is a hybrid system which uses an 8-kG NdFeB permanent magnet as a dispersive element, followed by a second, 5-kG NdFeB magnet to provide redundant energy determination by measuring the electron's track curvature through multiple detector planes. The spatial resolution for locating a track's coordinates at each emulsion plane is <2 μm, and the eventual resolution of the reconstructed energy is $\sim$20% at 1 GeV, limited by multiple scattering in the emulsion planes. The spectrum of electron energies is obtained by counting the number of individual tracks in a specified microscopic field of view at several locations along the dispersion plane, and converting the track densities to absolute differential cross sections. The energy dispersion (i.e.,
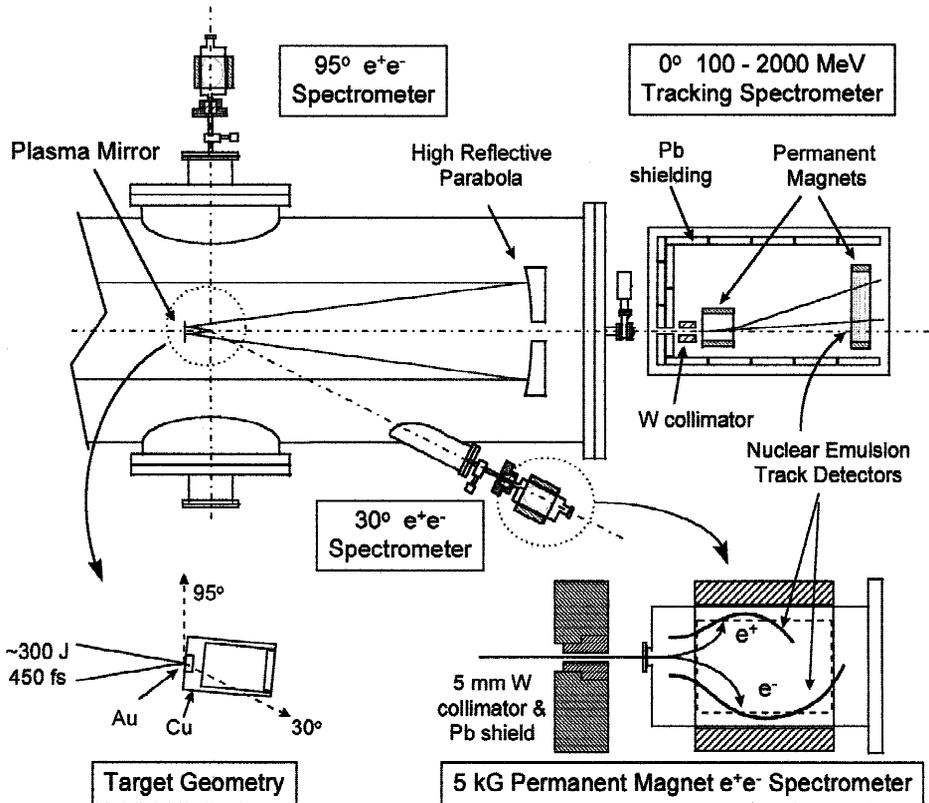
FIGURE 1. Schematic of the petawatt target chamber and electron spectrometers. The compressed laser beam enters from the left, is reflected from the $f = 180$-cm parabola to a secondary plasma mirror, and reflected onto the target at the chamber center. The high energy spectrometer (at right) measures electrons (~ 100–2000 MeV) emitted near $0°$, which pass through a hole in the parabola. Low energy spectrometers measure electrons (0.2–140 MeV) and positrons (0.2–40 MeV) emitted at $30°$ and $\sim 95°$ from the target (lower right).

position *versus* energy) was calculated by ray tracing and confirmed by calibration measurements performed at the LLNL 100-MeV electron Linac.

The first high energy electron spectra measured on the petawatt are shown in figure 2, from an experiment in September 1997 to characterize the high-energy bremsstrahlung X-ray yield in short pulse solid target interactions (Perry 1998a). The target was a 0.5-mm-thick, 2-mm-diameter disk of Au, mounted in the end plate (~ 0.5-mm-thick) of a cylindrical Cu can (subsequent targets in this shot series were thicker). As shown in figure 1, the laser light was focused using a secondary plasma mirror in a Cassegranian geometry. The total laser energy incident on the Au target was ~ 280 J, with a pulse duration of 450 fs. The energy enclosed in the central focal spot was sufficient to achieve a focused intensity of $\sim 8 \times 10^{19}$ W/cm^2.

Two important features of these data are the large excess of 5–15 MeV electrons observed in the forward direction, and the presence of a very high energy tail extending to above 80 MeV in both spectra. The forward enhancement of the electron angular distribution is even larger than it appears because those electrons detected in the $30°$ spectrometer had to penetrate the target. In so doing, they lost substantial energy ($\Delta E \sim 2.5$ MeV for minimum ionizing particles) and were multiply scattered through rather large angles. Monte–Carlo electron transport calculations suggest that the forward electron flux between 2–15 MeV may be an order of
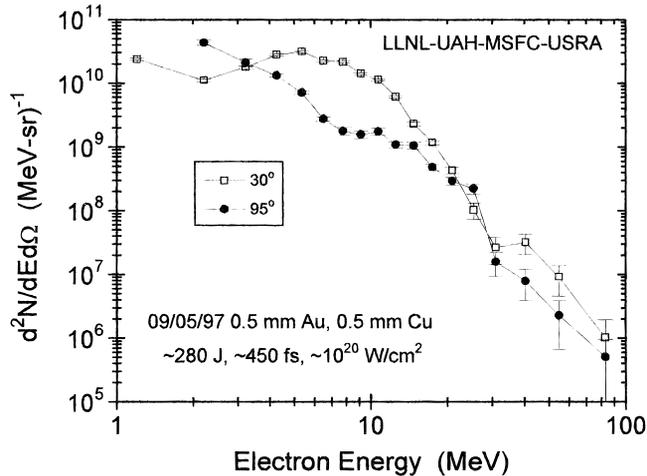
FIGURE 2. Distribution of electrons measured in magnetic spectrometers at 30° (open) and 95° (solid), from the first short-pulse (0.5 ps) petawatt shot series on 5 September 1997. The 0.5-mm Au target was backed by 0.5-mm Cu. The estimated incident laser energy was 280 J, delivered in 450 ± 50 fs, with an estimated focused intensity of 8×10^{19} W/cm^2.

magnitude or more larger than the factor of ~ 10 enhancement already apparent from figure 2. The low energy portion of the electron spectrum at both angles is also suppressed, compared to the actual energy distribution of electrons present in the target plasma, due to a large, $\sim$few MV space charge potential which develops as electrons are expelled from the focus during the laser pulse. Because the laser pulse duration is so short, the return current of electrons flowing from the bulk of the target material does not have time to fully neutralize the positive space charge potential formed by the current of ejected relativistic electrons.

Including reasonable estimates of the above effects, the lower energy portion of these spectra, up to ~ 20 MeV, appear reasonably consistent with the expected Maxwellian distribution having a mean energy of ~ 3 MeV, predicted from equation (1), at the nominal intensity of $\sim 10^{20}$ W/cm^2. However, the presence of the high energy tail in each spectrum out to nearly 100 MeV, indicates a more complicated laser-target interaction. The laser prepulse in this experiment is estimated to have preformed a ~ 50-μm scale length plasma at the surface of the Au target, sufficient to cause either selffocusing of the laser light to much higher intensity, or selfmodulated laser plasma acceleration (Wilks 1998; Hatchett 1998).

3. Photon-neutron reactions and transmutation

The presence of very energetic electrons in the forward directed spectrum in figure 2 suggests the generation of a substantial flux of hard bremsstrahlung X rays produced by the passage of the relativistic electrons through the Au target. The portion of the bremsstrahlung spectrum above the threshold for photonuclear reactions should contribute to photoneutron emission from the Au and Cu and, if sufficiently intense, produce measurable long lived activities in the target. Immediately following each laser shot, the target assemblies were measured with a high resolution HPGe gamma ray spectrometer to identify the specific daughter nuclides present. A typical gamma ray energy spectrum for an activated target is shown in figure 3. The production of ^{196}Au nuclei by ^{197}Au$(\gamma, n)^{196}$Au is clearly identified by the appearance of the nuclear deexcitation gamma rays in the ^{196}Pt daughter nuclide at 356 keV and 333 keV. In addition, the less probable β^- decay of ^{196}Au to ^{196}Hg is also identified by the line
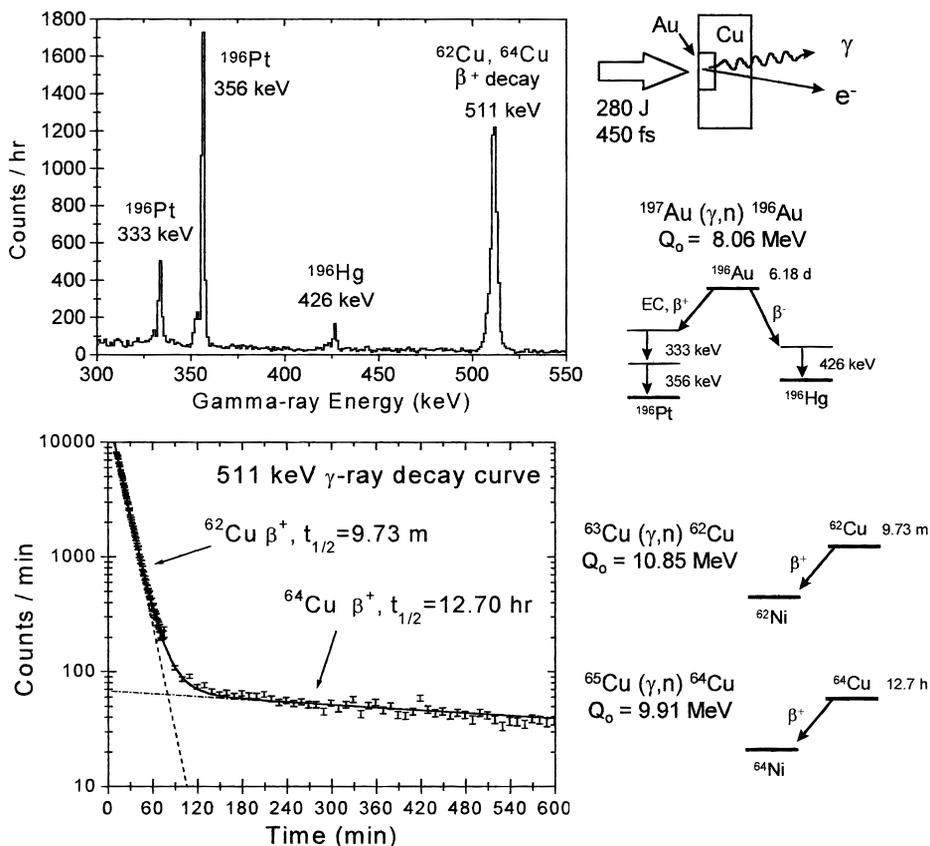
FIGURE 3. Photoneutron activation of Au and Cu target material in an intense petawatt laser shot. (Upper left) gamma ray energy spectrum measured with a high purity Ge detector. Peaks correspond to nuclear deexcitation gamma rays following decay of ^{196}Au to ^{196}Pt and ^{196}Hg (see decay scheme at right). (Lower left) Count rate *versus* time for the 511 keV gamma ray peak from positron annihilation following $\beta+$ decay of ^{62,64}Cu to ^{62,64}Ni. Curves show two component fit of exponential decay corresponding to the half lives for the $\beta+$ decay of ^{62}Cu and ^{64}Cu.

at 426 keV. The intensities of the 333, 356, and 426 keV gamma ray lines were observed to exhibit a decay rate consistent with the 6.18 day half-life of the ^{196}Au parent, confirming their identification.

The measurable yield of ^{197}Au$(\gamma,n)\,^{196}$Au reactions indicates a large flux of bremsstrahlung photons above the threshold energy for this reaction of $Q_0 = 8.06$ MeV. Photoneutron activation of the principal Cu isotopes by the reactions ^{65}Cu$(\gamma,n)\,^{64}$Cu$(Q_0 = 9.91$ MeV$]$, and ^{63}Cu$(\lambda,n)\,^{62}$Cu$(Q_0 = 10.85$ MeV$]$ are also observed by the beta decay of their neutron deficient daughters to ^{64}Ni and ^{62}Ni respectively. These were identified in this experiment by the 511 keV positron-annihilation gamma ray line, whose decay curve shown in figure 3 reveals two principal components whose decay constants match the 9.7 min and 12.7-hr half-lives of ^{62}Cu and ^{64}Cu, respectively. In this first high intensity laser-solid experiment, we therefore identified three photo-neutron reactions in Au and Cu produced from the laser-target interaction. We believe that their subsequent radioactive decays to isotopes of platinum, mercury and nickel represent the first observations of the transmutation of an element from a laser produced plasma (Cowan 1998a).

From the total activation yield of each nuclide, and using the known $\sigma_{\gamma,n}$ nuclear cross sections, one may estimate the total flux of bremsstrahlung photons above the threshold energy Q_0 emitted into the forward hemisphere (i.e., intercepting the bulk of the target material) (Cowan 1998a; Key 1998; Perry 1998a; Phillips 1998). For example, the $^{63}Cu(\gamma,n)^{62}Cu$ activation yield implies a total forward-going flux of $\sim 10^{11}$ photons above 10.85 MeV, for the data of figure 2.

4. High energy photon measurements

The above (γ,n) reactions in Au, and additional photonuclear reactions in Ni, are now being used as powerful diagnostics of the high energy electron and bremsstrahlung flux generated in each shot (Phillips 1998). The choice of Au and Ni as activation targets gives a maximum spread of (γ,n) threshold energies among the elements for which the photon energy dependence of the cross sections are well known, and together allow an accurate determination of the exponential slope of the high energy bremsstrahlung distribution above ~ 8 MeV. Most recently, nuclear activation is being used to determine the spatial distribution of the high energy bremsstrahlung, by including in each of the Cu target sample holders an array of Au pellets (Sangster 1998). The necessity of obtaining sufficient activation in each pellet to obtain statistically reasonable activation yields limits the smallest feasible pellet size ($\sim$mm).

The high energy sensitivity of the Au activation technique complements a companion effort to determine the angular distribution of the generated X-ray pattern using a large array of thermo-luminescent dosimeters (Snavely 1998). The TLDs have a much lower threshold response of ~ 250 keV (determined primarily by the geometry and thickness of Ta filter material surrounding the TLD). Due to the broad, exponential nature of the electron and bremsstrahlung energy distributions, the TLD technique tends to preferentially sample the lower energy, ponderomotive-like portion of the energy distribution, whereas the nuclear activation techniques sample the higher energy portion of the spectrum assumed to be associated more with electron acceleration in the underdense and near-critical density portion of the preformed plasma at the target.

Solid state diodes, encased in 2.5 cm of lead, have been used to increase the threshold response to ~ 1 MeV photon energies, and provide quantitatively similar results to the TLD measurements (Moran 1998). Using additional or varying composition of filter material to further adjust the photon threshold response becomes quite difficult in this energy range because for most elements one is near the Compton minimum, for which the mass-attenuation coefficient is essentially constant with photon energy. The determination of the photon energy response of both diodes and TLDs in an actual measurement geometry is further complicated by the electron-photon shower which develops in the attenuating filter materials, in addition to the less directional secondary radiation generated as the electrons and photons from the target strike the chamber walls and either scatter or generate additional tertiary radiations.

In an attempt to measure the intervening range of photon energies (~ 2–8 MeV), where neither the activation nor direct photon absorption techniques work well, we have tried unsuccessfully to use photo-dissociation of deuterium with the measurement of the neutron energy distribution by time-of-flight techniques (Key 1998). In fact, the present sample holder was designed to contain a CD_2 cylinder of sufficient size to provide an easily measurable neutron yield in the NOVA large area neutron scintillator array. In the first short pulse (0.5 ps) petawatt experiments, it came somewhat as a surprise that the electron and bremsstrahlung spectra extended to such high energy, and the deuterium photo-dissociation neutrons could not be distinguished from the huge flux of photo-neutrons coming from high energy (γ,n) reactions in the Au target, Cu can, and Al chamber walls. Calculations of the total neutron yield (Hatchett 1998) from all of these sources, based on the measured electron spectra and predicted bremsstrahlung distribution, are in good agreement with measurements of the quasi-isotropic neu-

tron flux made by neutron capture spectroscopy (Singh 1998). In light of these complexities, we are evaluating additional photonuclear techniques (for example, photofission) to directly access photon energies below the 8-MeV Au (γ, n) threshold (Hunt 1998).

5. Observation of jet-like phenomena

The eventual usefulness of ultra intense laser plasma interactions as single-state high-gradient accelerators or as radiation sources for nuclear physics and other fundamental or applied investigations requires some degree of control and reproducibility. In this experimental campaign, a total of eight target shots were accumulated for which basic features of the electron energy distribution in figure 2, in particular the presence of the high energy electron tail, and the photoneutron activation discussed above, were quite similar. The overall electron and activation yields are summarized in figure 4. It should be noted that the seven later targets were somewhat thicker (2 mm Au, 2 mm Cu) than the first, which further attenuated the low energy portion of the electron spectrum measured in the 30° spectrometer (figure 5a). Apart from this systematic difference, and a marked reversal of the electron angular distribution on the sixth shot, the yield data are well correlated, particularly the forward electron and the activation yields which are, respectively, the source for, and the result of, the bremsstrahlung produced in the target.

Most of the order-of-magnitude, shot-to-shot variation in the yields is attributable to variations in the laser pulse energy and focal aberrations caused by pump-induced thermal distortions in the NOVA Nd:glass amplifiers. This has been solved in recent experiments by an adaptive optics system which successfully corrects for these distortions on a given shot by preconfiguring a deformable mirror based on the wavefront data in a Hartmann sensor accumulated on prior shots (Perry 1998b). These remains, however, residual shot-to-shot variations particularly in the directionality of the radiation pattern. Recent measurements indicate that the maximum position of the angular distribution of the $\sim$MeV X rays can shift dramatically from
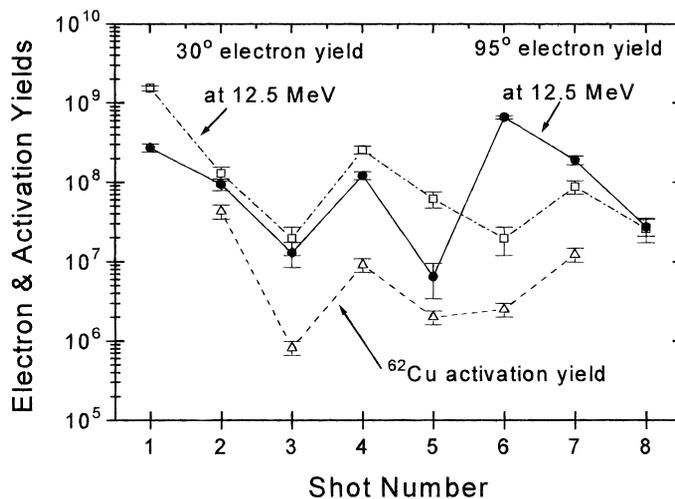

FIGURE 4. Comparison of electron and activation yields for the eight petawatt target shots in this experiment. The curves plot the electron differential cross section $(\mathrm{MeV}^{-1}\,\mathrm{sr}^{-1})$, measured in the 30° and 95° spectrometers, at a fixed electron energy of 12.5 MeV. The activation curve plots the number of ^{62}Cu nuclei produced in the target assembly, calculated from the time $= 0$ intercept of the fitted ^{62}Cu decay curve from figure 3, corrected for the 511 keV full-energy-peak detection efficiency in the high purity Ge gamma ray spectrometer.
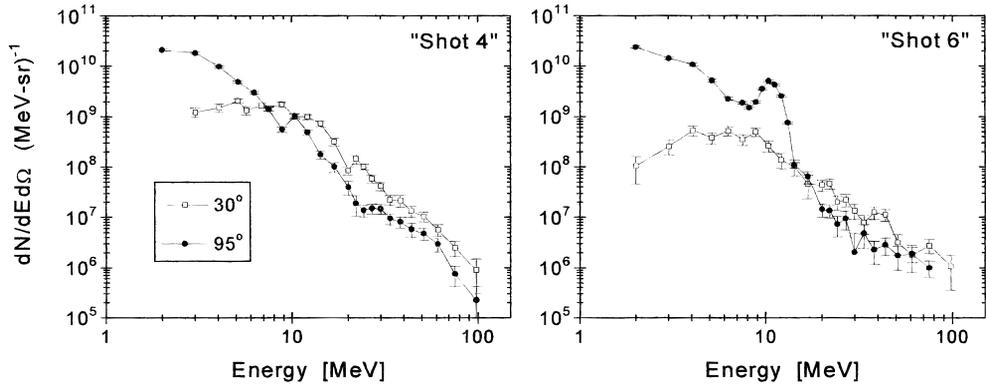
FIGURE 5. Electron spectra for shots 4 and 6. Note the thicker target in shots 2–8 further attenuates the measured electron distribution in the forward, 30° spectrometer (compare figure 2). Electron spectra of shot 4 are typical of most other shots. Shot 6 exhibits a decrease in forward directed electron flux below 20 MeV, and a well defined peak in the transverse directed electron distribution at 10.75 MeV.

shot to shot (Perry 1998b; Snavely 1998). Similar effects have been reported from ICF experiments on the GEKKO 100 TW laser at Osaka (Tanaka 1998). Several groups have noted a dependence of the yield of hard X-ray generation on laser prepulse and preformed plasma conditions in lower energy laser experiments (Malka 1996). Most probably, spatial nonuniformities in the preformed plasma lead to laser filamentation and/or self focusing with some degree of directional instability. The presence of exceptionally strong magnetic fields ($\sim$10 MG) generated by the ponderomotive electron current in the overcritical portion of the target might induce additional beaming and kinking (Lasinski 1998). It should be emphasized in this respect that the underdense plasma formation is so far accomplished with a prepulse in advance of, and under the same focal conditions, as the high intensity beam. LASNEX calculations indicate that the pre-formed plasma scale length is expected to be comparable to the focal spot size (Hatchett 1998), and will exhibit complex structure associated with focal aberrations.

Even more complicated laser-plasma effects appear also to be important in these experiments as shown by the extreme deviation of the electron energy and angle distribution on isolated shots. As shown in figure 5, for example, in addition to a general shifting of electron intensity from the forward to transverse directions on the sixth shot of the September 1997 series, a remarkably narrow enhancement in the energy spectrum of electrons at 95° is observed at 10.75 MeV, having a FWHM of $\sim$2.5 MeV. Repeated, independent scans of the emulsion strip, at different positions within the projected image of the entrance aperture, verify the statistical reproducibility and significance of the peak-like feature. Although the origin of this jet-like feature in energy is at present unknown, it is presumably associated with some aspect of the evolution of the plasma at the target vacuum interface. If controllable, it could have future usefulness as a high current, short pulse electron beam source for radiation generation.

6. Positron production

Finally, we present preliminary evidence for the production of positron-electron pairs in the ultra intense, laser matter interactions in the petawatt solid-target shots. The yield of positron–electron pairs under our experiment conditions is expected to be of order 10^{-4} of the electron yield observed at 30°, in the energy range 5–10 MeV. The nuclear emulsion track detection of such rare events, both because of its intrinsic single particle detection sensitivity, and because

of the relative immunity of emulsions to the intense high energy X ray flux generated in relativistic laser interactions at and above the critical plasma density. As noted in section 2, the electron energy spectrum in figure 2 was derived from spot inspection of the electron track density in the exposed emulsion, at several points along the dispersion plane. The typical electron track density at 10 MeV was of order 10^5 per cm^2, which corresponded to 10^2 of order tracks identified, under microscopic examination, within each 500-μm-diameter field of view.

The sparse nature of the positron data, however, did not require spot scanning, but a complete scan of the entire emulsion strip, with critical attention paid to the quality and characteristics of each track to avoid spurious misidentification of scattered background events. This painstaking analysis was performed in a double-blind fashion, with the human scanners not informed of the total yield or spatial distribution of true positron signal tracks, which was to be expected in this exposure. Similarly, the calculations of background processes have been performed without knowledge of the observed yield and distribution of tracks. The positron candidates are identified by satisfying three criteria—the track grain density, the incident angle, and the transverse position of the track with respect to the dispersion plane. As scattered high energy electrons would also have the same grain density as the minimum-ionizing positrons, the spatial and angle distributions are of key importance in distinguishing between positrons emitted from the target and background scatter. The entrance angle distribution is in fact quite narrow, and is determined from the projected track length on an event-by-event basis. The spatial distribution within the emulsion detector strip was the decisive information required to assess signal *versus* background rates. As shown in figure 6, we found that most events fell within the projected image of the entrance aperture along the detector plane. Of the 103 candidate events, we independently estimated that <3 were due to external conversion backgrounds in the spectrometer material, and estimated a signal between 50 and 200 events, based on preliminary estimates of the bremsstrahlung photon distribution in the target material. Assuming that all candidates represent signal from the target site, we present the derived energy distribution of positron events between 3 and 9 MeV, compared to the electron data from this shot (figure 2). The relative intensity of positron to electron yield is of order 10^{-4}, consistent with expectations.

Although positron production is not surprising, given the presence of high energy bremsstrahlung produced in these laser-solid experiments, this measurement does represent the first observation of the conversion of pure laser energy into antimatter. The E-144 experiment at SLAC (see, e.g, Meyerhofer 1997) has previously observed positron-electron pair production from an ultrarelativistic electron beam interaction with a low energy, short pulse laser. Although much more interesting in terms of the fundamental quantum electrodynamics under investigation in that experiment, the source of energy for the materialization of the pair was an artifact of the Lorentz boost into the rest of the frame beam, and therefore was extracted primarily from the kinetic energy of the incident electrons. In this case, the energy source is the incident laser beam, and in a sense represents the conversion (albeit inefficient and indirect) of ~eV photons from the laser to ~MeV photons (bremsstrahlung), followed by energy-to-mass conversion as well as the previously described nuclear excitations and reactions.

7. Summary

In summary, we have begun to explore a new regime of laser-matter interactions where the electron quiver energies are well above the threshold for causing nuclear reactions. In first petawatt class laser-solid target experiments, we have observed a high energy component in the electron spectrum, up to ~100 MeV, in addition to a forward-directed, lower energy distribution which appears to be consistent with the relativistic dynamics of the electrons in the laser focus at the nominal focused intensities of ~10^{20} W/cm^2. High energy bremsstrahlung produced in the Au targets was observed to produce photoneutron reactions in the Au target and Cu
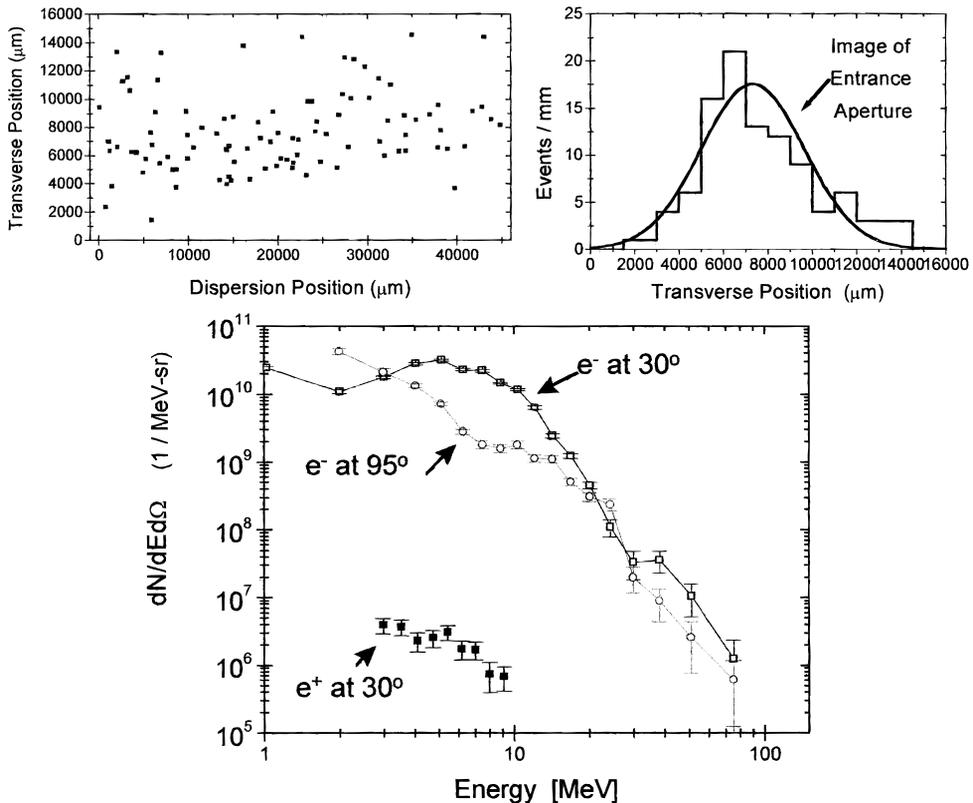
FIGURE 6. Distribution of candidate positron tracks in an emulsion detector plane, measured in the 30° spectrometer on the shot of fig. 2. Histogram of track positions transverse to the dispersion plane, consistent with the projected image of the entrance aperture. Energy distribution of positrons measured between 3 and 9 compared to electron spectra from the same shot (see fig. 2). Predicted ratio of positron to electron production is $\sim 10^{-4}$, consistent with these data.

sample-holder material. The production of radioactive isotope daughters, and their subsequent decay to stable isotopes of Pt, Hg, and Ni, to our knowledge represents the first observation of laser-assisted transmutation of elements. Furthermore, we have evidence for the first observation of positron production in laser-plasma interactions (Cowan 1998c). Subsequent experiments have revealed evidence for higher energy photoneutron reactions, up to $(\gamma, 5n)$, indicating bremsstrahlung photon energies above 40 MeV (Sangster 1998), and the first observation of laser-fission (Hunt 1998). Residual shot-to-shot variations in the energy and angular distributions of electron and bremsstrahlung yields appear to be associated with variable preformed plasma conditions which are not yet under strict experimental control. Future developments will include controlling the performed plasma conditions by eliminating the laser prepulse and by implementing a separately timed and focused preform beam.

Acknowledgments

REFERENCES

COWAN, T.E. *et al.* 1997 In *Applications of High Field and Short Wavelength Sources VII*, (OSA Technical Digest Series) Vol. 7, p. 243.

COWAN, T.E. *et al.* 1998a In *Proceedings of the International Conference on Lasers '97*, J.J. Carroll & T.A. Goldman, eds., STS Press, McLean Va), pp. 882–889.

COWAN, T.E. *et al.* 1998b In *Proceedings of the 8th Workshop on Advanced Accelerator Concepts* (J. Lawson, ed., AIP Press).

COWAN, T.E. *et al.* 1998c "Relativistic Electron and Positron Production in Petawatt Laser-Solid Interactions" (to be published).

COWAN, T.E. *et al.* 1998d "Design and performance of a magnetic electron and positron spectrometer using nuclear emulsion track detection" (to be published).

HATCHETT, S. *et al.* 1998 (to be published). See also PERRY *et al.* 1998a.

HUNT, A.W. *et al.* 1998a "Laser Fission" (to be published).

KEY, M.H. *et al.* 1998a *Phys. Plasmas* **5**, 1966.

LASINSKI, B. & LANGDON A.B. 1998 (to be published). See also [PERRY 1998b].

MEYER-TER-VEHN *et al.* 1998 *XXVth ECLIM*, *Laser and Particle Beams* (these proceedings).

PERRY, M.D. *et al.* 1996 *Science and Technology Review* (Lawrence Livermore National Laboratory, UCRL-52000-96-12), p. 12.

PERRY, M.D. *et al.* 1998a "Hard X-ray production from high intensity laser solid interactions," *Rev. Sci. Instrum.* (to be published).

PERRY, M.D. *et al.* 1998b (to be published).

PHILLIPS, *et al.* 1998a "Diagnosing hot electron production by short pulse, high intensity lasers using photonuclear reactions," *Rev. Sci. Instrum.* (to be published).

PUKOV, A. *et al.* 1998 *XXVth ECLIM*, *Laser Particle Beams* (these proceedings).

MALKA, G. & MIQUEL J.L. 1996 *Phys. Rev. Lett.* **77**, 75.

MEYERHOFER, D.D. *et al.* 1996, *Phys. Rev. Lett.* **76**, 3116.

MORAN, M.J. 1998 (to be published). See also [KEY 1998].

SNAVELY, R.A. 1998 (to be published). See also [PERRY 1998b].

SANGSTER, T.C. *et al.* 1998 (to be published).

SINGH, M.S. *et al.* 1998 (to be published). See also [PERRY 1998a].

TANAKA, K.A. *et al.* 1998 *XXVth ECLIM*, *Lasers Particle Beams* (these proceedings).

WILKS, S.C. 1992 *Phys. Rev. Lett.* **69**, 1383.

WILKS, S.C., & KRUER, W.L. 1998 (to be published).